Detecting gravitational waves sources – BHBH, NSNS, BHNS – with LISA

Nazeela Aimen, Syed Ali Mohsin Bukhari, Asad Ali

Department of Applied Mathematics and Statistics, Institute of Space Technology, Islamabad 44000, Pakistan.

Space and Astrophysics Research Lab (SARL), Institute of Space Technology, Islamabad 44000, Pakistan.

Abstract

Abstract is still missing!!

Index Terms

Cobb-Douglas Habitability Score, Exoplanets, Habitability, Habitable zone, Convex Optimization, Duality.

I. Introduction

The gravitational waves (GW) were predicted a year after the final formulation of the general theory of relativity (GR) by Albert Einstein [1]. Similar to electromagnetic waves, the GWs travel at the speed of light [2, 3]. However, unlike electromagnetic waves, the GW stretches and squeezes the space itself thus causing spatial disturbances. The detection of Hulse-Taylor binary [4], and the subsequent observation of a seven years time span [5] stirred a great interest in the GW observations. It wasn't until 2015 that the first direct observation of GW was made by LIGO and VIRGO collaborations [3]. The lower frequency bound for both the aLIGO and VIRGO detectors is around $10\,\mathrm{Hz}$ [6, 7]

The Laser Interferometer Space Antenna (LISA) has three spacecrafts that form a triangle, each side 2.5 million km long [8, 9]. Operating in the frequency range of $1 \times 10^{-5}\,\mathrm{Hz} \leq f \leq 1 \times 10^{-1}\,\mathrm{Hz}$ LISA will be able to observe the sources millions of years before they merge. The early detection capability will help better constrain and determine the orbital parameters of the observed binaries. Some sources detectable by LISA are the extreme mass ratio inspirals (EMRIs) [10, 11, 12] and galactic binaries [3, 13, 14]. This makes LISA also capable of mapping Milky Way galaxy's structure. Another interesting class detectable by LISA is the double white dwarf stars (DWDs) which are reported to be abundant in our MW galaxy and have a substantial detection in LISA as well [15, 16, 17, 18].

A lot of effort has been put into the detection of potential GW sources for LISA, the resolution of issues that might be associated with the background data, and proposals of new candidates as GW sources for LISA [see, for example, 13, 16, 18, 19, 20, 21, 22, 23, 24, 25, 26, 27, 28, 29, 30, 31, 32]. The detections of these sources will provide us with a better understanding of not only the evolution phases but also the endpoints of stellar evolution.

The goals of this research are,

- to predict the number of DCO binaries that can be detected via LISA in our Milky Way galaxy,
- to determine whether extra galactic sources are LISA detectable,
- to make a general detection comparison between DCO binaries with and without an initial eccentricity.

For this purpose, we generate the binaries using COMPAS, section II. One hundred random Milky Way (MW) instances were generated in which the binaries were placed for detection, section B. The detection of the binaries was done using LEGWORK v0.3.0 [33].[1]

[1] https://github.com/TeamLEGWORK/LEGWORK/tree/v0.3.0

II. Population synthesis

The population synthesis for the detections of the double compact objects (DCOs) was performed using the Compact Object Mergers: Population Astrophysics and Statistics (COMPAS; [34, 35, 36]) suite. COMPAS is a rapid stellar evolution suite and can evolve both single and binary stars following the details outlined by [37, 38]. A list of selected papers that make use of the COMPAS suite is also available on the COMPAS website.[2]

This study makes use exclusively of the binary star evolution (BSE) synthesis method. The default parameters used by the COMPAS software are listed in table 1 in the COMPAS paper [35].

Except for supernova mass remnant prescription, initial eccentricity (e_i), metallicity (z), and pulsar evolution, all other parameters were taken at the default value. For a one-to-one correspondence between the two generated data sets, the seed numbers were kept constant.

For the mass of primary star, we draw the values from Kroupa initial mass function (IMF) with $m_1 \in [5, 150]\,\mathrm{M}_\odot$ [39]. For the secondary star, we randomly draw from uniform distribution to satisfy $q \equiv m_2/m_1$, where $q \in [0, 1]$ [40]. An additional constraint of $m_2 \geq 0.1\,m_1$ was placed on m_2 as this is the minimum mass necessary for a star to be considered as a main sequence star.

For the semi-major axis of the binary, we drew the parameter values from a flat-in-the-log distribution with $a_i \in [0.1, 1000]$ AU, such that $p(a_i) \propto 1/a_i$ [41].

For the remnant mass prescription, we first considered the Fryer delayed model [42]. However, this resulted in a concentration of NS mass around $\sim 1.28\,\mathrm{M}_\odot$. To avoid this concentration of NS final mass, we used Müller & Mandel prescription (M&M) [43]. M&M is a stochastic remnant mass model that offers a smoother mass distribution for NS. We also switched the **evolve_pulsar** flag to **True** during population synthesis.

For metallicity, we drew the values from a $\mathrm{Beta}(5, 80)$ distribution. The main motivation behind the selection of such biased distribution is the higher metallic content of present-day stars. The population III stars were primarily composed of pure hydrogen and their deaths produced heavier metals in the Universe. By this extension, the stars that are present now or those that will merge now must have higher metallic content. As such, we also note that having stars with higher metallic content might produce more NSNS or NS-BH pairs for detection.

For eccentricity, we make use of two cases,

- Case I: All the binary systems are generated using a flat distribution, $e \in [0, 1]$.
- Case II: All the binary systems are generated with circular orbits, i.e., $e = 0$.

Details about the selection of metallicity and eccentricity values in COMPAS are provided in appendix A. In section IV we discuss the summary of the DCOs formed by the COMPAS generated binaries. In addition to the parameter mentioned above, the COMPAS chooses four more parameters stochastically. Including kick random magnitude, kick phi, kick theta, and kick mean anomaly.

III. Parameters of interest

We first generated 1×10^7 values for metallicity using the beta distribution within the COMPAS limits (see, appendix A for details). We denote the zero-age main sequence (ZAMS) parameters of the binaries as,

$$m_{1_{\mathrm{ZAMS}}}, m_{2_{\mathrm{ZAMS}}}, a_{\mathrm{ZAMS}}, e_{\mathrm{ZAMS}}, Z, \varnothing \tag{1}$$

COMPAS evolves the binaries up to $13.7\,\mathrm{Gyr}$. We represent the resulting double compact object (DCO) parameters as,

$$m_{1_{\mathrm{DCO}}}, m_{2_{\mathrm{DCO}}}, a_{\mathrm{DCO}}, e_{\mathrm{DCO}}, t_{\mathrm{evolve}}, t_{\mathrm{inspiral}}, Z, \varnothing, \tag{2}$$

where Z is the metallicity of the binary system, $\varnothing$ is the seed number, t_{evolve} is the time required to form DCO from ZAMS, and t_{inspiral} is the DCO in-spiral time. a_{ZAMS}, a_{DCO}, e_{ZAMS}, and e_{DCO} are the semi-major axis and eccentricity of the binary orbit at ZAMS and DCO formation respectively. These parameters were

[2] https://compas.science/science.html

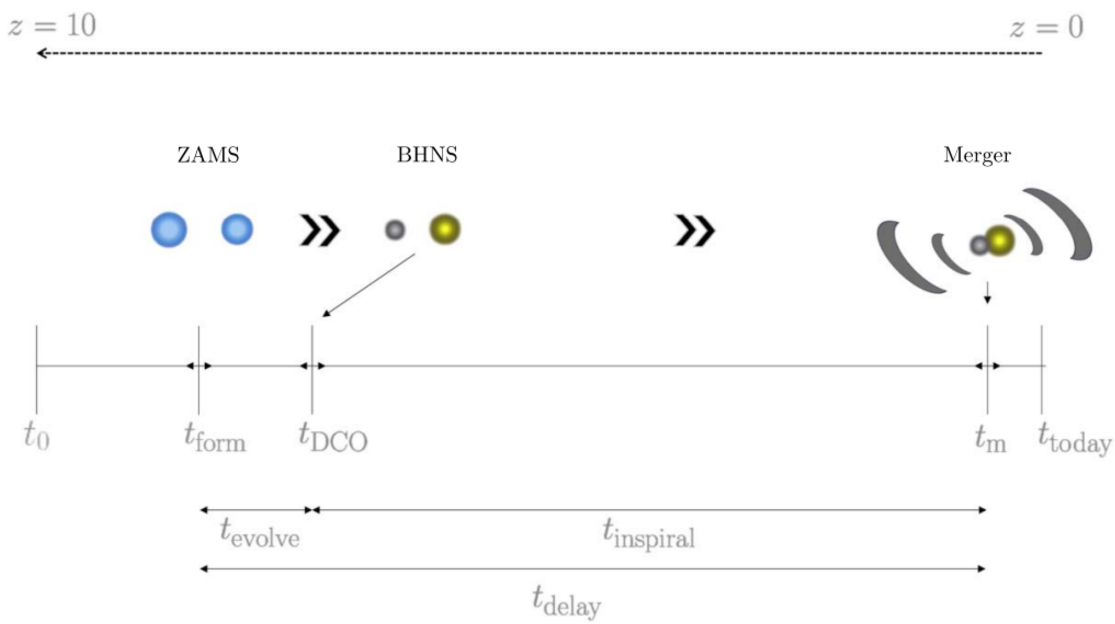

Fig. 1: Schematic diagram showing various time intervals for a binary system from ZAMS formation, to DCO, and merger. The figure is taken from [35].

then provided to the python framework LEGWORK [33] that evolved these binaries from the DCO stage to the merger state. It evolves the binaries using equations from [44, 45]. The detection is made based on the signal-to-noise ratio (SNR) of the binary averaged over sky position, polarization, and orientation using the following expression from [46],

$$\rho^2 = \sum_{n=1}^{\infty} \int_{f_{n,i}}^{f_{n,f}} \frac{h_{c,n}^2}{f_n^2 S_n(f_n)} \, \mathrm{d}f_n, \tag{3}$$

where n is the GW harmonic, f_n represents the orbital frequency of $n^{\rm th}$ harmonic. The parameter $S_n(f_n)$ is the LISA sensitivity curve function [9], and $h_{c,n}$ is the characteristic strain of the $n^{\rm th}$ GW harmonic [47].

$$h_{c,n}^2 = \frac{2^{5/3}}{3\pi^{4/3}} \frac{(G\mathcal{M}_c)^{5/3}}{c^3 D_L^2} \frac{1}{f_{\rm orb}^{1/3}} \frac{g(n,e)}{nF(e)} \tag{4}$$

The DCO-merger evolution method follows the one outlined by [13] closely. The evolution was done such that the MW galaxy instance was divided into bins based on the metallicity values of the evolving binaries. The evolution time was calculated after taking into consideration the ZAMS-DCO evolution time and the lookback time of the binary produced. If a binary, at DCO stage, had a resultant merger time greater than the difference of its lookback time and ZAMS-DCO evolution time, it was marked as an inspiralling binary. Each inspiralling binary was than evolved at every point within the corresponding metallicity bin using LEGWORK to a million year before its merger time. At this stage, the resulting LISA parameters of interest were,

$$a_{\rm LISA}, e_{\rm LISA}, f_{\rm LISA} \tag{5}$$

The SNR was than calculated by further evolving them for the LISA mission duration of four or ten years. As the number of binaries detected in our study is small compared to the total generated population[3], multiple detections of a single binary object are present in the output.

[3] Due to not using any technique that forces DCO produciton, e.g., STROOPWAFEL [48]

IV. Results

After running the simulations following section II, we obtained 12254 DCOs ($\sim 0.12254\%$). Out of these, only 6539 DCOs merged within Hubble time (∼53.3622%) thus making them a potential LISA source.[4] The formation rate of DCOs is given in table I,

BHBH	NSNS	BHNS	
		NSBH	BHNS
492/663	4752/9219	480/663	815/1504

TABLE I: Number of DCOs merged within Hubble time vs total DCOs formed by the COMPAS suite.

Overall, in this study, the highest merging rate is of BHBH DCO type ($\sim 74.21\%$), followed by NSBH ($\sim 72.4\%$), BHNS ($\sim 54.2\%$) and lastly NSNS DCO type ($\sim 51.55\%$).

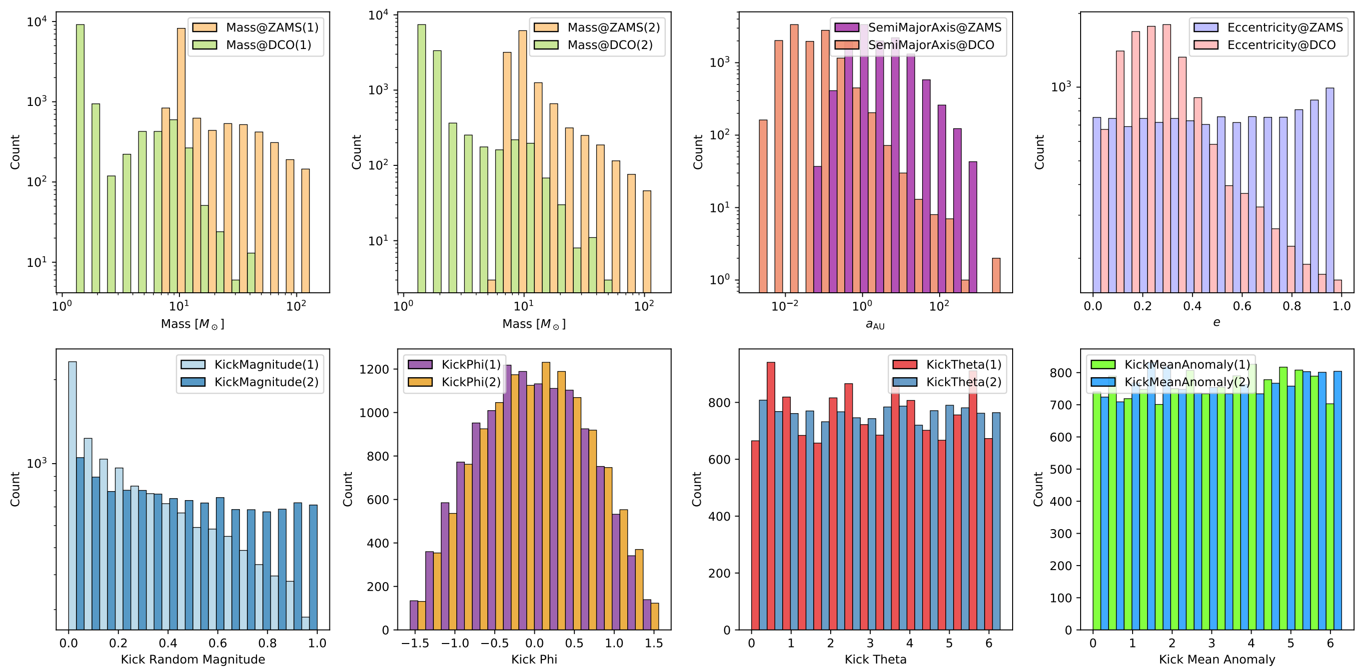

Fig. 2: The top row shows the distribution of mass, semimajor axis and eccentricity of binary pairs at ZAMS and DCO stage for the merged DCO binaires. The bottom row shows the selection of supernova kick paramters made by the COMPAS suite.

A. Binary black holes

We now consider the BHBH population

This section contains our findings and results, comprising the predictions of the given types of DCOs for LISA in the Milky Way and a detailed analysis of their properties. Based on our fiducial model, we expect in total $4.7 \times 10^{-3}\% \, (186.41)$ detections on average in a $4 \, (10)$ years LISA mission in which $1.39 \times 10^{-3}\% \, (108.35)$, $1.4 \times 10^{-3}\% \, (6.68)$, $1.91 \times 10^{-3}\% \, (34.94)$ are BHBH, NSBH, and NSNS respectively. Moreover, we also plot our detectable sources concerning the LISA sensitivity curve (figure 3a) in section IV-B. **Tell the summary of the rest of the results here.**

While this section comprises detailed analysis of our fiducial model, section V describes the comparison of eccentricity-based simulations.

[4]Overall, only ∼0.06539% binary system formed into DCOs that merge within Hubble time.

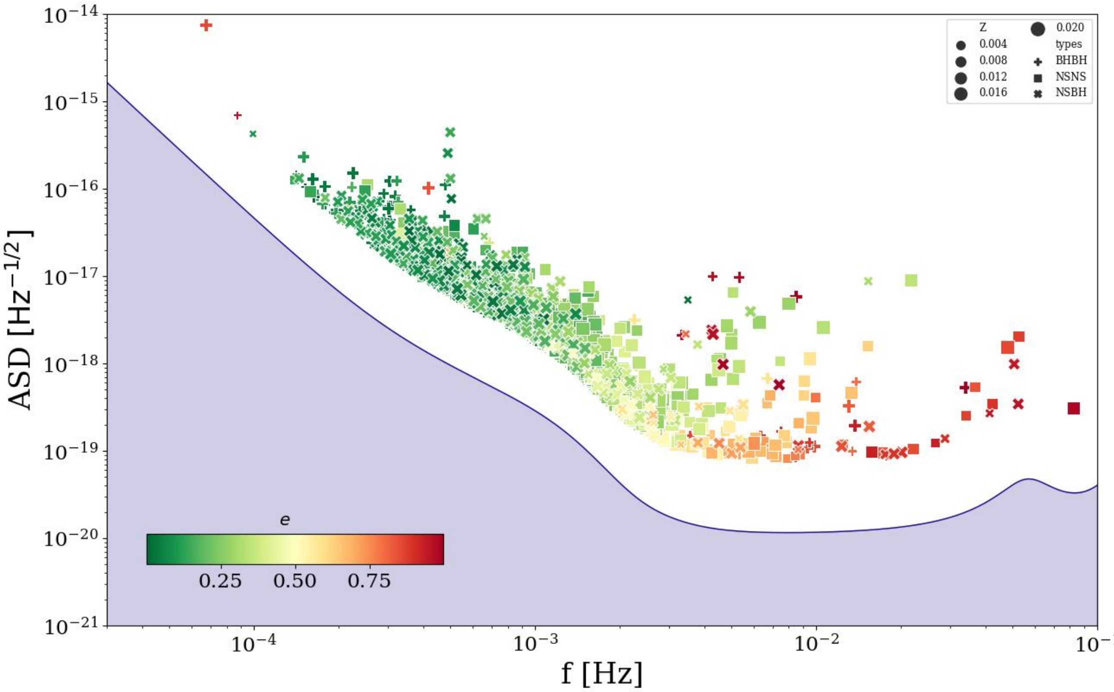

Fig. 3a: Detectable sources' characteristic strain along with dominant frequency in our simulations (Top) is shown on the LISA sensitivity curve as well as their separate types (bottom). The sources are placed based on their eccentricities i.e. Highly eccentric sources are towards the red side while low eccentric sources are on the green side of the spectrum. The reference lines are based on the average eccentricity of our simulations i.e. where in the galaxy an eccentric binary would be assuming an average chirp mass, orientation, and sky location for a remaining inspiral time (vertical lines) and a given distance (diagonal lines). See also figure bla bla for detail understanding.

B. Population of Detectable sources

The predicted distribution of the LISA detectable sources is plotted over its expected sensitivity curve, containing the galactic double white dwarf population noise [9], in figure 3a. The x-axis of the graph is the GW frequency. For the circular binaries in our data, the GW frequency is $2f_{\mathrm{orb}}$ is the correspondence for the x-axis. We take the dominant frequency, the frequency accumulating the largest SNR, for the eccentric binaries. Furthermore, the y-axis stipulates the amplitude spectral density (ASD), including the contribution from all harmonics.

The gap between the detected binaries and the LISA curve in the graph is the SNR criteria, (SNR > 7). Furthermore, the binaries are shaped based on their type; plus, square, and cross show BHBH, NSBH, and NSNS, respectively. The size of the points varies with metallicity; high metallic sources have larger shapes than low metallic ones. The color scheme for the binaries is based on the eccentricity strength of the detected binaries, shown through a color bar at the bottom left in the plot. For example, the red ones are the most eccentric sources, the yellow ones are mid-eccentric, and the green ones are the sources with low eccentricities.

Around $3\,$mHz, some binaries mostly have large eccentricities. These are on the right side of the graph and extend downwards to 10^{-19} ASDs. However, there are also some BHBH that are almost circular and emit at high frequency. These sources are in their last stages of merger hence they are spinning fast enough to emit large frequency GW.

The major binary population is concentrated on the left side of the LISA sensitivity curve. The peak of concentration around the GW frequency of **0.12 mHz**. The main reason for such a trend can be explained through the eccentricities of the binaries. As seen from the figure 3a, a large population of our binaries

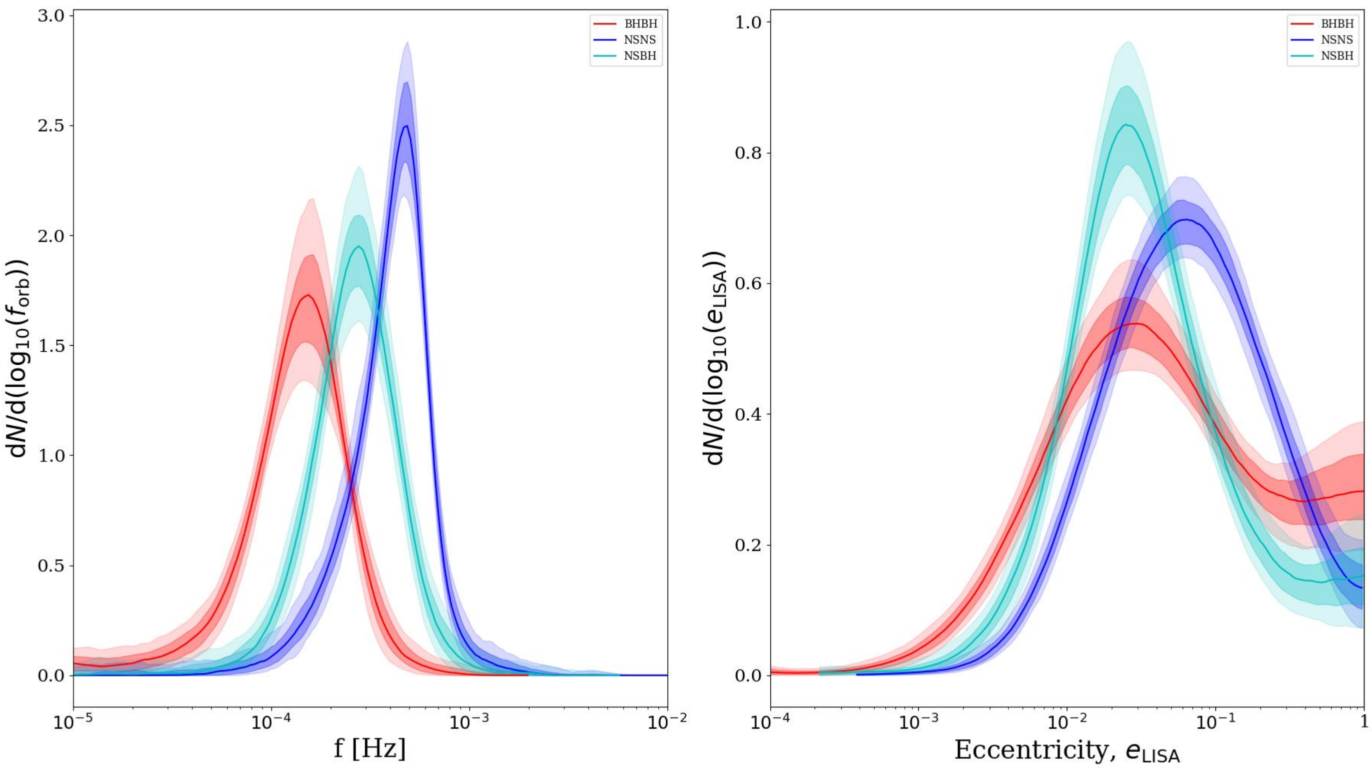

Fig. 3b: Caption text.

are low eccentric or mid-eccentric. There are also binaries having high eccentricities which as mentioned above lie on the right side of the graph. The orbit of low eccentric or circular binaries evolves differently than high eccentric binaries. After the formation of DCO, most of the low eccentric binaries emit GW in low-frequency bands of LISA as the orbit progresses. While DCOs with high eccentricities behave in a completely different way, i.e. their orbit decay faster, and they tend to emit GW in the high-frequency LISA detection band. Although these are of prime importance in the LISA mission, unfortunately, these are rare. Thus, most of the DCOs are at lower frequency regions.

Fig. 3b shows the distribution of the orbital frequency; f, and eccentricity at the time of LISA mission; e. The regions surrounding the individual graphs are the $1\,\sigma$, and $2\,\sigma$ uncertainties which are the variations of the results over 100 random instances of our galaxy. We plot this figure using the bootstrapping function [13]. The left side of the graph is the orbital frequency distribution. It shows peaks of different types of sources i.e. **0.3mHz, 0.7mHz, 0.99** for BHBH, NSNS, and NSBH. The reason for such a trend is because of the mass difference as higher mass DCO The distribution is a little negatively skewed. As mentioned above, a higher mass DCO at the same distance and eccentricity requires a lower frequency to produce the same signal-to-noise ratio and thus be detected. The orbital frequency distributions for BHBHs, BHNSs, and NSNSs (figure, 3a) peak at progressively increasing frequencies as mentioned in section 3.1. The distributions appear nearly symmetric, but closer inspections show that the left-hand side is more populated, which can be seen most clearly in the curve for the BHBHs. This is due to the contribution of highly eccentric binaries, which are most abundant in the BHBH population. These systems are still detectable by LISA, despite their low orbital frequency, as the high eccentricity means that the majority of the GW signal is emitted at higher harmonics, where LISA is more sensitive.

We can also observe the peaks for high chirp mass systems have peaks in the low-frequency detection region, as they emit the waves in lower frequency. Hence, this is another way to differentiate sources. Hence, the BHBH pairs have the most eccentric pairs having the highest average eccentricity and $\langle M_c \rangle$.

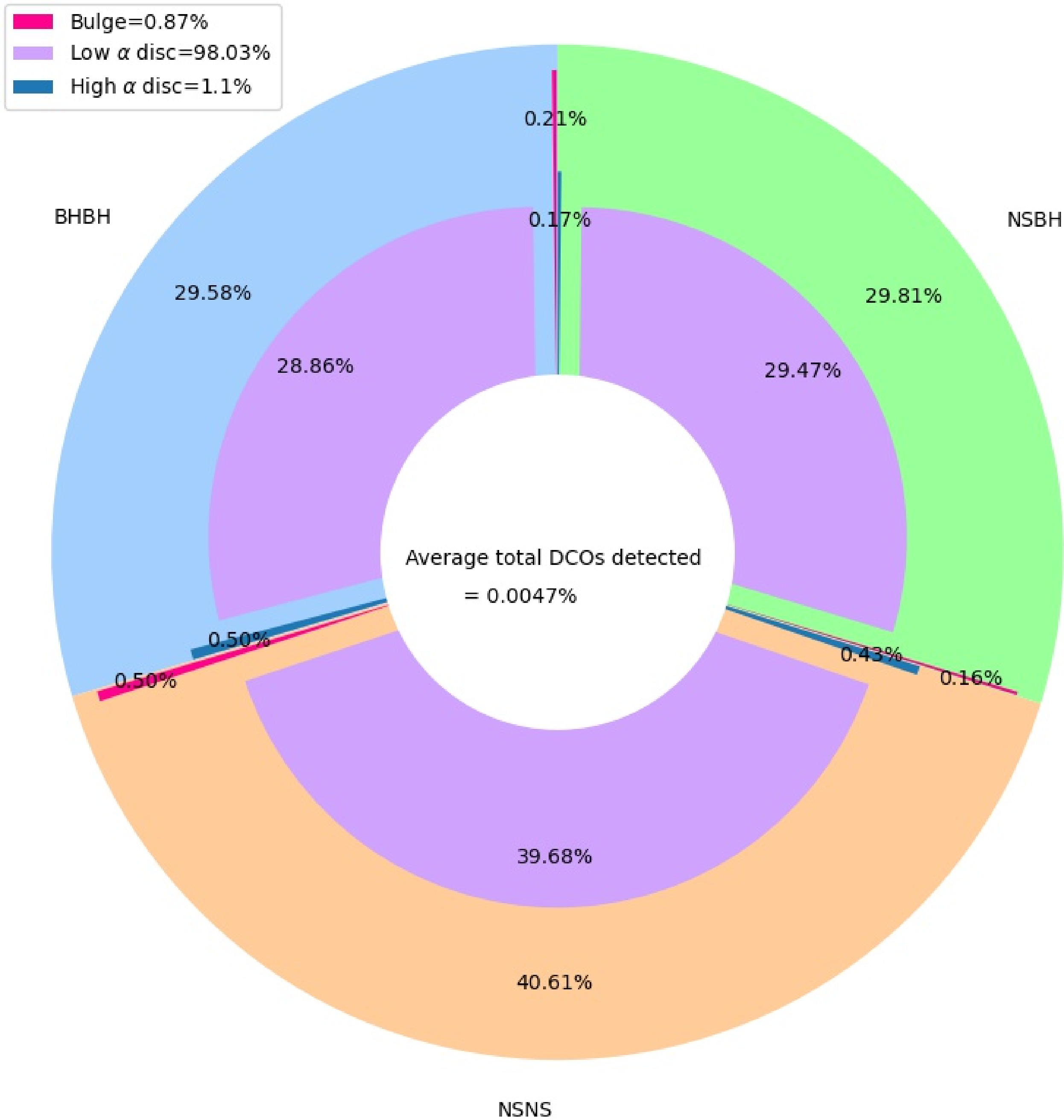

Fig. 4: Average detectable sources distribution in three components of simulated milky way

C. Detections in Components

Our simulated galaxy comprises three components; Low α disc, High α disc, and Bulge. Figure 4 describes the average distribution of detectable sources in these components. The average total number of detections are in shown in the middle. BHBH, having a significant number of detections, is equally distributed in the low$-\alpha$ disc and high$-\alpha$ disc, while the rest have slightly more detections in the latter than prior. Bulge has the least number of detected DCOs. Thus, there is a high probability for LISA to detect GW sources in the two components.

D. Maximum distance

For each DCO, there is a horizon distance i.e., the maximum distance up to which the DCO may be detectable in LISA. This is calculated using the inverse relationship between SNR (ρ) and distance [19],

$$d_{\text{max}} = \frac{\rho(d\,=\,1\,\text{kpc})}{\rho_{\text{min}}} \tag{6}$$

Where ρ_{min} is the minimum value of SNR below which the source is not detectable. We keep the detection threshold at $\rho_{\text{min}} = 7$, and $\rho(d = 1\,\text{kpc})$ is SNR of the source if it was at $1\,\text{kpc}$ distance from the detector. We calculated the SNR of all the detected sources at $1\,\text{kpc}$ distance using the python package LEGWORK [33]. Afterward, their maximum distances (d_{max}) were calculated.

Figure 5 shows the maximum distances for all the detected sources. The top shows d_{max} for BHBH, and NSNS while the bottom has NSBH and BHNS. These are calculated for all the LISA band frequencies. The black line shows the average maximum distance for all the types. The LISA sensitivity curve is also overlaid on the graph as a blue line.

BHBH, being the dominant source can be observed to an average distance of more than $1 \times 10^5\,\text{kpc}$. NSBH and BHNS have almost the same average d_{max} i.e between $1 \times 10^3\,\text{kpc}$ and $1 \times 10^4\,\text{kpc}$ while NSNS has peak at $\sim 1 \times 10^3\,\text{kpc}$. The red dotted lines illustrate some known galaxies to have a better understanding of distances. Hence, BHBH can be discovered as far as Hoag's Object, NSNS in M31, and both BHNS and NSBH are far from M31 but much below Hoag's Object.

Almost all the highest values of average d_{max} of four types are around a **certain frequency** i.e., if a source has **certain orbital frequency** then it can be detected to its maximum detection distance. It can be observed through the LISA overlay that this frequency lies in the area where the detector is most sensitive. Hence, if a source emits in the frequency region of the highest sensitivity of LISA, then it will be detected at a maximum distance.

V. Results 2: Influence of Eccentricity

In this section, the outcomes of varying eccentricity at ZAMS are discussed. For this we use the same grid of parameters used in the fiducial model, however, the eccentricity is taken 0 at ZAMS (E0) instead of variable (VE).

Firstly, the detection rates and predictions for different sources are discussed. Afterward, changes in observable properties are discussed.

A. Detection rates

The prediction for VE is a total of 136 detections in a 4 years LISA mission. A decrease in the detection rate is observed for E0 which is detected in a 4 years LISA mission. As there is no difference in any parameter other than eccentricity, then it is surely the root cause of the decline in detections.

The difference in different types of sources is shown in the pie chart in which there is a clear reduction in the detected sources. **Explain the pie chart more**

B. Model variation: To be added somewhere else,

In a number of previous works, e_{ZAMS} was taken as zero [13, 19, 24, 36, 49]. The main reason for this assumption is that they argue that eccentricity at ZAMS is not likely critical for predicting detection rates as they deal with post-interaction binaries and their orbital eccentricities become zero after mass transfer [38]. To test the accuracy of this assumption, we simulate another population with the same parameters. The only change is that e_{ZAMS} of the binaries is left to be varied by the COMPAS suite. We compare the difference in detection rates and properties of the two models and give our conclusion.

VI. Discussion and Future work

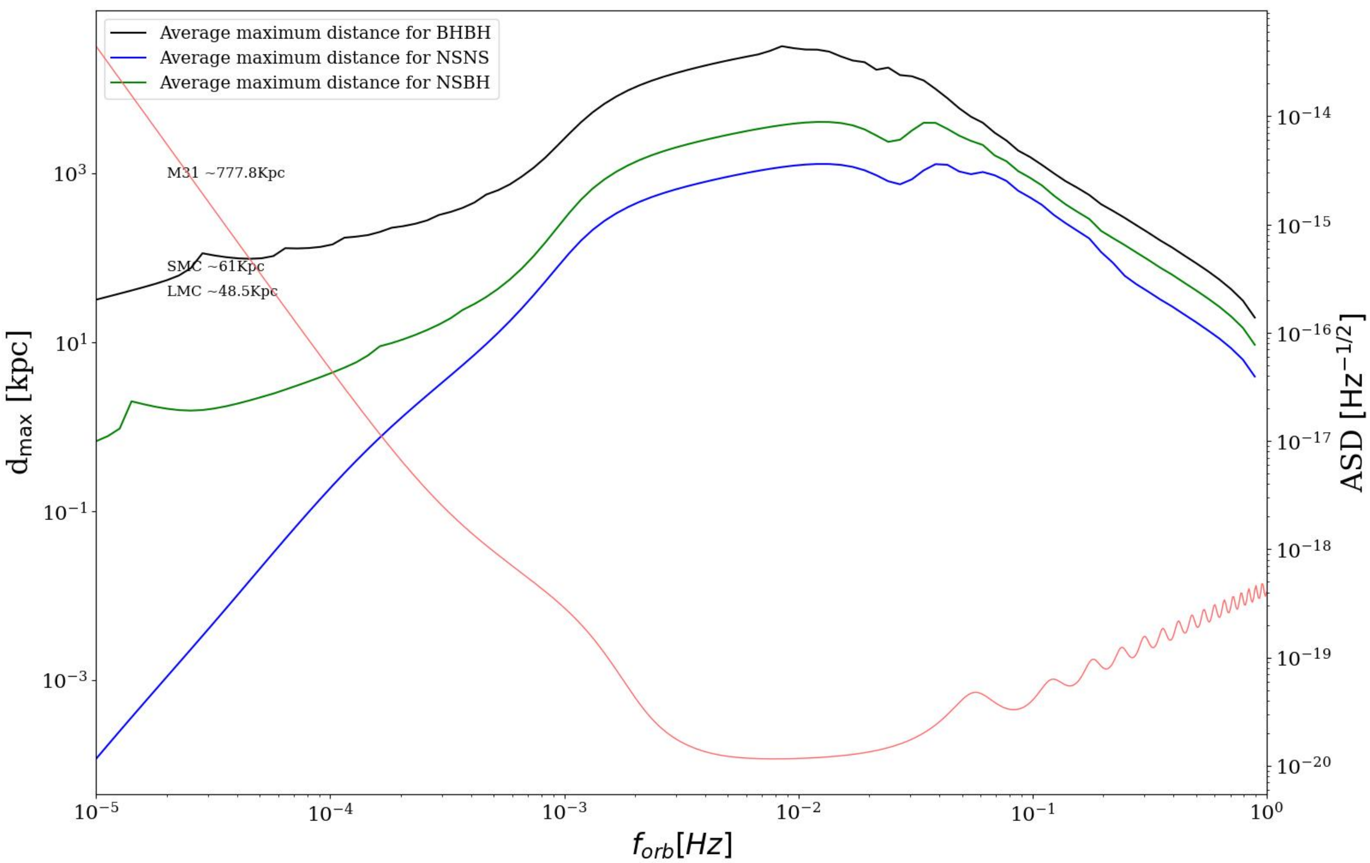

Fig. 5: Maximum distances for all of the different types of DCO. The average maximum distance is shown through a black line while the blue line shows the overlaid LISA sensitivity curve

References

[1] A. Einstein, "Näherungsweise Integration der Feldgleichungen der Gravitation," *Sitzungsberichte der Königlich Preußischen Akademie der Wissenschaften (Berlin)*, pp. 688–696, Jan. 1916.

[2] A. S. Eddington, "The Propagation of Gravitational Waves," *Proceedings of the Royal Society of London Series A*, vol. 102, no. 716, pp. 268–282, Dec. 1922.

[3] B. P. Abbott, R. Abbott, T. D. Abbott, F. Acernese, K. Ackley, C. . Adams, T. Adams, P. Addesso, R. X. Adhikari, V. B. Adya, C. Affeldt, M. Afrough, B. Agarwal, M. Agathos, K. Agatsuma, N. Aggarwal, O. D. Aguiar, L. Aiello, A. Ain, P. Ajith, B. Allen, G. Allen, A. Allocca, M. A. Aloy, P. A. Altin, A. Amato, A. Ananyeva, S. B. Anderson, W. G. Anderson, S. V. Angelova, S. Antier, S. Appert, K. Arai, M. C. Araya, J. S. Areeda, N. Arnaud, K. G. Arun, S. Ascenzi, G. Ashton, M. Ast, S. M. Aston, P. Astone, D. V. Atallah, P. Aufmuth, C. Aulbert, K. AultONeal, C. Austin, A. Avila-Alvarez, S. Babak, P. Bacon, M. K. M. Bader, S. Bae, P. T. Baker, F. Baldaccini, G. Ballardin, S. W. Ballmer, S. Banagiri, J. C. Barayoga, S. E. Barclay, B. C. Barish, D. Barker, K. Barkett, F. Barone, B. Barr, L. Barsotti, M. Barsuglia, D. Barta, J. Bartlett, I. Bartos, R. Bassiri, A. Basti, J. C. Batch, M. Bawaj, J. C. Bayley, M. Bazzan, B. Bécsy, C. Beer, M. Bejger, I. Belahcene, A. S. Bell, B. K. Berger, G. Bergmann, J. J. Bero, C. P. L. Berry, D. Bersanetti, A. Bertolini, J. Betzwieser, S. Bhagwat, R. Bhandare, I. A. Bilenko, G. Billingsley, C. R. Billman, J. Birch, R. Birney, O. Birnholtz, S. Biscans, S. Biscoveanu, A. Bisht, M. Bitossi, C. Biwer, M. A. Bizouard, J. K. Blackburn, J. Blackman, C. D. Blair, D. G. Blair, R. M. Blair, S. Bloemen, O. Bock, N. Bode, M. Boer, G. Bogaert, A. Bohe, F. Bondu, E. Bonilla, R. Bonnand, B. A. Boom, R. Bork, V. Boschi, S. Bose, K. Bossie, Y. Bouffanais, A. Bozzi, C. Bradaschia, P. R. Brady, M. Branchesi, J. E. Brau, T. Briant, A. Brillet, M. Brinkmann, V. Brisson, P. Brockill, J. E. Broida, A. F. Brooks, D. A. Brown, D. D. Brown, S. Brunett, C. C. Buchanan, A. Buikema, T. Bulik, H. J. Bulten, A. Buonanno, D. Buskulic, C. Buy, R. L. Byer, M. Cabero, L. Cadonati, G. Cagnoli, C. Cahillane, J. Calderón Bustillo, T. A. Callister, E. Calloni, J. B. Camp, M. Canepa, P. Canizares, K. C. Cannon, H. Cao, J. Cao, C. D. Capano, E. Capocasa, F. Carbognani, S. Caride, M. F. Carney, J. Casanueva Diaz, C. Casentini, S. Caudill, M. Cavaglià, F. Cavalier, R. Cavalieri, G. Cella, C. B. Cepeda, P. Cerdá-Durán, G. Cerretani, E. Cesarini, S. J. Chamberlin, M. Chan, S. Chao, P. Charlton, E. Chase, E. Chassande-Mottin, D. Chatterjee, K. Chatziioannou, B. D. Cheeseboro, H. Y. Chen, X. Chen, Y. Chen, H. P. Cheng, H. Chia, A. Chincarini, A. Chiummo, T. Chmiel, H. S. Cho, M. Cho, J. H. Chow, N. Christensen, Q. Chu, A. J. K. Chua, S. Chua, A. K. W. Chung, S. Chung, G. Ciani, R. Ciolfi, C. E. Cirelli, A. Cirone, F. Clara, J. A. Clark, P. Clearwater, F. Cleva, C. Cocchieri, E. Coccia, P. F. . Cohadon, D. Cohen, A. Colla, C. G. Collette, L. R. Cominsky, J. Constancio, M., L. Conti, S. J. Cooper, P. Corban, T. R. Corbitt, I. Cordero-Carrión, K. R. Corley, N. Cornish, A. Corsi, S. Cortese, C. A. Costa, M. W. Coughlin, S. B. Coughlin, J. P. Coulon, S. T. Countryman, P. Couvares, P. B. Covas, E. E. Cowan, D. M. Coward, M. J. Cowart, D. C. Coyne, R. Coyne, J. D. E. Creighton, T. D. Creighton, J. Cripe, S. G. Crowder, T. J. Cullen, A. Cumming, L. Cunningham, E. . Cuoco, T. Dal Canton, G. Dálya, S. L. Danilishin, S. D'Antonio, K. Danzmann, A. Dasgupta, C. F. Da Silva Costa, V. Dattilo, I. Dave, M. Davier, D. Davis, E. J. Daw, B. Day, S. De, D. DeBra, J. Degallaix, M. De Laurentis, S. Deléglise, W. Del Pozzo, N. Demos, T. Denker, T. Dent, R. De Pietri, V. Dergachev, R. De Rosa, R. T. DeRosa, C. De Rossi, R. DeSalvo, O. de Varona, J. Devenson, S. Dhurandhar, M. C. Díaz, L. Di Fiore, M. Di Giovanni, T. Di Girolamo, A. Di Lieto, S. Di Pace, I. Di Palma, F. Di Renzo, Z. Doctor, V. Dolique, F. Donovan, K. L. Dooley, S. Doravari, I. Dorrington, R. Douglas, M. Dovale Álvarez, T. P. Downes, M. Drago, C. Dreissigacker, J. C. Driggers, Z. Du, M. Ducrot, P. Dupej, S. E. Dwyer, T. B. Edo, M. C. Edwards, A. Effler, H. B. Eggenstein, P. Ehrens, J. Eichholz, S. S. Eikenberry, R. A. Eisenstein, R. C. Essick, D. Estevez, Z. B. Etienne, T. Etzel, M. Evans, T. M. Evans, M. Factourovich, V. Fafone, H. Fair, S. Fairhurst, X. Fan, S. Farinon, B. Farr, W. M. Farr, E. J. Fauchon-Jones, M. Favata, M. Fays, C. Fee, H. Fehrmann, J. Feicht, M. M. Fejer, A. Fernandez-Galiana, I. Ferrante, E. C. Ferreira, F. Ferrini, F. Fidecaro, D. Finstad,

I. Fiori, D. Fiorucci, M. Fishbach, R. P. Fisher, M. Fitz-Axen, R. Flaminio, M. Fletcher, H. Fong, J. A. Font, P. W. F. Forsyth, S. S. Forsyth, J. D. Fournier, S. Frasca, F. Frasconi, Z. Frei, A. Freise, R. Frey, V. Frey, E. M. Fries, P. Fritschel, V. . V. Frolov, P. Fulda, M. Fyffe, H. Gabbard, B. U. Gadre, S. M. Gaebel, J. R. Gair, L. Gammaitoni, M. R. Ganija, S. G. Gaonkar, C. Garcia-Quiros, F. Garufi, B. Gateley, S. Gaudio, G. Gaur, V. Gayathri, N. Gehrels, G. Gemme, E. Genin, A. Gennai, D. George, J. George, L. Gergely, V. Germain, S. Ghonge, A. Ghosh, A. Ghosh, S. Ghosh, J. A. Giaime, K. D. Giardina, A. Giazotto, K. Gill, L. Glover, E. Goetz, R. Goetz, S. Gomes, B. Goncharov, G. González, J. M. Gonzalez Castro, A. Gopakumar, M. L. Gorodetsky, S. E. Gossan, M. Gosselin, R. Gouaty, A. Grado, C. Graef, M. Granata, A. Grant, S. Gras, C. Gray, G. Greco, A. C. Green, E. M. Gretarsson, P. Groot, H. Grote, S. Grunewald, P. Gruning, G. M. Guidi, X. Guo, A. Gupta, M. K. Gupta, K. E. Gushwa, E. K. Gustafson, R. Gustafson, O. Halim, B. R. Hall, E. D. Hall, E. Z. Hamilton, G. Hammond, M. Haney, M. M. Hanke, J. Hanks, C. Hanna, M. D. Hannam, O. A. Hannuksela, J. Hanson, T. Hardwick, J. Harms, G. M. Harry, I. W. Harry, M. J. Hart, C. J. Haster, K. Haughian, J. Healy, A. Heidmann, M. C. Heintze, H. Heitmann, P. Hello, G. Hemming, M. Hendry, I. S. Heng, J. Hennig, A. W. Heptonstall, M. Heurs, S. Hild, T. Hinderer, D. Hoak, D. Hofman, K. Holt, D. E. Holz, P. Hopkins, C. Horst, J. Hough, E. . A. Houston, E. J. Howell, A. Hreibi, Y. M. Hu, E. A. Huerta, D. Huet, B. Hughey, S. Husa, S. H. Huttner, T. Huynh-Dinh, N. Indik, R. Inta, G. Intini, H. . N. Isa, J. M. Isac, M. Isi, B. R. Iyer, K. Izumi, T. Jacqmin, K. Jani, P. Jaranowski, S. Jawahar, F. Jiménez-Forteza, W. W. Johnson, N. . K. Johnson-McDaniel, D. I. Jones, R. Jones, R. J. G. Jonker, L. Ju, J. Junker, C. V. Kalaghatgi, V. Kalogera, B. Kamai, S. Kandhasamy, G. Kang, J. B. Kanner, S. J. Kapadia, S. Karki, K. S. Karvinen, M. Kasprzack, W. Kastaun, M. Katolik, E. Katsavounidis, W. Katzman, S. Kaufer, K. Kawabe, F. Kéfélian, D. Keitel, A. J. Kemball, R. Kennedy, C. Kent, J. S. Key, F. Y. Khalili, I. Khan, S. Khan, Z. Khan, E. A. Khazanov, N. Kijbunchoo, C. Kim, J. C. Kim, K. Kim, W. Kim, W. S. Kim, Y. M. Kim, S. J. Kimbrell, E. J. King, P. J. King, M. Kinley-Hanlon, R. Kirchhoff, J. S. Kissel, L. Kleybolte, S. Klimenko, T. D. Knowles, P. . Koch, S. M. Koehlenbeck, S. Koley, V. Kondrashov, A. Kontos, M. Korobko, W. Z. . Korth, I. Kowalska, D. B. Kozak, C. Krämer, V. Kringel, B. Krishnan, A. Królak, G. Kuehn, P. Kumar, R. Kumar, S. Kumar, L. Kuo, A. Kutynia, S. . Kwang, B. D. Lackey, K. H. Lai, M. Landry, R. N. Lang, J. Lange, B. Lantz, R. K. Lanza, A. Lartaux-Vollard, P. D. Lasky, M. Laxen, A. Lazzarini, C. Lazzaro, P. Leaci, S. Leavey, C. H. Lee, H. K. Lee, H. M. Lee, H. W. Lee, K. Lee, J. Lehmann, A. Lenon, M. Leonardi, N. Leroy, N. Letendre, Y. Levin, T. G. F. Li, S. D. Linker, T. B. Littenberg, J. Liu, R. K. L. Lo, N. A. Lockerbie, L. T. London, J. E. Lord, M. Lorenzini, V. Loriette, M. Lormand, G. Losurdo, J. D. Lough, C. O. Lousto, G. Lovelace, H. Lück, D. Lumaca, A. P. Lundgren, R. Lynch, Y. Ma, R. Macas, S. Macfoy, B. Machenschalk, M. MacInnis, D. M. Macleod, I. Magaña Hernandez, F. Magaña-Sandoval, L. Magaña Zertuche, R. M. Magee, E. Majorana, I. Maksimovic, N. Man, V. Mandic, V. Mangano, G. L. Mansell, M. Manske, M. Mantovani, F. Marchesoni, F. Marion, S. Márka, Z. Márka, C. Markakis, A. S. Markosyan, A. Markowitz, E. Maros, A. Marquina, F. Martelli, L. Martellini, I. W. Martin, R. M. Martin, D. V. Martynov, K. Mason, E. Massera, A. Masserot, T. J. Massinger, M. Masso-Reid, S. Mastrogiovanni, A. Matas, F. Matichard, L. Matone, N. Mavalvala, N. Mazumder, R. McCarthy, D. E. McClelland, S. McCormick, L. McCuller, S. C. McGuire, G. McIntyre, J. McIver, D. J. McManus, L. McNeill, T. McRae, S. T. McWilliams, D. Meacher, G. D. Meadors, M. Mehmet, J. Meidam, E. Mejuto-Villa, A. Melatos, G. Mendell, R. A. Mercer, E. L. Merilh, M. Merzougui, S. Meshkov, C. Messenger, C. Messick, R. Metzdorff, P. M. Meyers, H. Miao, C. Michel, H. Middleton, E. E. Mikhailov, L. Milano, A. L. Miller, B. B. Miller, J. Miller, M. Millhouse, M. C. Milovich-Goff, O. Minazzoli, Y. Minenkov, J. Ming, C. Mishra, S. Mitra, V. P. Mitrofanov, G. Mitselmakher, R. Mittleman, D. Moffa, A. Moggi, K. Mogushi, M. Mohan, S. R. P. Mohapatra, M. Montani, C. J. Moore, D. Moraru, G. Moreno, S. R. Morriss, B. Mours, C. M. Mow-Lowry, G. Mueller, A. W. Muir, A. Mukherjee, D. Mukherjee, S. Mukherjee, N. Mukund, A. Mullavey, J. Munch, E. A. Muñiz, M. Muratore, P. G. Murray, K. Napier, I. Nardecchia, L. Naticchioni, R. K. Nayak, J. Neilson,

G. Nelemans, T. J. N. Nelson, M. Nery, A. Neunzert, L. Nevin, J. M. Newport, G. Newton, K. K. Y. Ng, T. T. Nguyen, D. Nichols, A. B. Nielsen, S. Nissanke, A. Nitz, A. Noack, F. Nocera, D. Nolting, C. North, L. K. Nuttall, J. Oberling, G. D. O'Dea, G. H. Ogin, J. J. Oh, S. H. Oh, F. Ohme, M. A. Okada, M. Oliver, P. Oppermann, R. J. Oram, B. O'Reilly, R. Ormiston, L. F. Ortega, R. O'Shaughnessy, S. Ossokine, D. J. Ottaway, H. Overmier, B. J. Owen, A. E. Pace, J. Page, M. A. Page, A. Pai, S. A. Pai, J. R. Palamos, O. Palashov, C. Palomba, A. Pal-Singh, H. Pan, H.-W. Pan, B. Pang, P. T. H. Pang, C. Pankow, F. Pannarale, B. C. Pant, F. Paoletti, A. Paoli, M. A. Papa, A. Parida, W. Parker, D. Pascucci, A. Pasqualetti, R. Passaquieti, D. Passuello, M. Patil, B. Patricelli, B. L. Pearlstone, M. Pedraza, R. Pedurand, L. Pekowsky, A. Pele, S. Penn, C. J. Perez, A. Perreca, L. M. Perri, H. P. Pfeiffer, M. Phelps, O. . J. Piccinni, M. Pichot, F. Piergiovanni, V. Pierro, G. Pillant, L. Pinard, I. M. Pinto, M. Pirello, M. Pitkin, M. Poe, R. Poggiani, P. Popolizio, E. K. Porter, A. Post, J. Powell, J. Prasad, J. W. W. Pratt, G. Pratten, V. Predoi, T. Prestegard, M. Prijatelj, M. Principe, S. Privitera, G. A. Prodi, L. . G. Prokhorov, O. Puncken, M. Punturo, P. Puppo, M. Pürrer, H. Qi, V. Quetschke, E. A. Quintero, R. Quitzow-James, F. J. Raab, D. S. Rabeling, H. Radkins, P. Raffai, S. Raja, C. Rajan, B. Rajbhandari, M. Rakhmanov, K. E. Ramirez, A. Ramos-Buades, P. Rapagnani, V. Raymond, M. Razzano, J. Read, T. Regimbau, L. Rei, S. Reid, D. H. Reitze, W. Ren, S. D. Reyes, F. Ricci, P. M. Ricker, S. Rieger, K. Riles, M. Rizzo, N. A. Robertson, R. Robie, F. Robinet, A. Rocchi, L. Rolland, J. G. Rollins, V. J. Roma, R. Romano, C. L. Romel, J. H. Romie, D. Rosińska, M. P. Ross, S. Rowan, A. Rüdiger, P. Ruggi, G. Rutins, K. Ryan, S. Sachdev, T. Sadecki, L. Sadeghian, M. Sakellariadou, L. Salconi, M. Saleem, F. Salemi, A. Samajdar, L. Sammut, L. M. Sampson, E. J. Sanchez, L. E. Sanchez, N. Sanchis-Gual, V. Sandberg, J. R. Sanders, B. Sassolas, B. S. Sathyaprakash, P. R. Saulson, O. Sauter, R. L. Savage, A. Sawadsky, P. Schale, M. Scheel, J. Scheuer, J. Schmidt, P. Schmidt, R. Schnabel, R. M. . S. Schofield, A. Schönbeck, E. Schreiber, D. Schuette, B. W. Schulte, B. F. Schutz, S. G. Schwalbe, J. Scott, S. M. Scott, E. Seidel, D. Sellers, A. S. Sengupta, D. Sentenac, V. Sequino, A. Sergeev, D. A. Shaddock, T. J. Shaffer, A. A. Shah, M. S. Shahriar, M. B. Shaner, L. Shao, B. Shapiro, P. Shawhan, A. Sheperd, D. H. Shoemaker, D. M. Shoemaker, K. Siellez, X. Siemens, M. Sieniawska, D. Sigg, A. D. Silva, L. P. Singer, A. Singh, A. Singhal, A. M. Sintes, B. J. J. Slagmolen, B. Smith, J. R. Smith, R. J. E. Smith, S. Somala, E. J. Son, J. A. Sonnenberg, B. Sorazu, F. Sorrentino, T. Souradeep, A. P. Spencer, A. K. Srivastava, K. Staats, A. Staley, M. Steinke, J. Steinlechner, S. Steinlechner, D. Steinmeyer, S. P. Stevenson, R. Stone, D. J. Stops, K. . A. Strain, G. Stratta, S. E. Strigin, A. Strunk, R. Sturani, A. L. Stuver, T. Z. Summerscales, L. Sun, S. Sunil, J. Suresh, P. J. Sutton, B. L. Swinkels, M. J. Szczepańczyk, M. Tacca, S. C. Tait, C. Talbot, D. Talukder, D. B. Tanner, M. Tápai, A. Taracchini, J. D. Tasson, J. A. Taylor, R. Taylor, S. V. Tewari, T. Theeg, F. Thies, E. G. Thomas, M. Thomas, P. Thomas, K. A. Thorne, K. S. Thorne, E. Thrane, S. Tiwari, V. Tiwari, K. V. Tokmakov, K. Toland, M. Tonelli, Z. Tornasi, A. Torres-Forné, C. I. Torrie, D. Töyrä, F. Travasso, G. Traylor, J. Trinastic, M. C. Tringali, L. Trozzo, K. W. Tsang, M. Tse, R. Tso, L. Tsukada, D. Tsuna, D. Tuyenbayev, K. Ueno, D. Ugolini, C. S. Unnikrishnan, A. L. Urban, S. A. Usman, H. Vahlbruch, G. Vajente, G. Valdes, N. van Bakel, M. van Beuzekom, J. F. J. van den Brand, C. Van Den Broeck, D. C. Vander-Hyde, L. van der Schaaf, J. V. van Heijningen, A. A. van Veggel, M. Vardaro, V. Varma, S. Vass, M. Vasúth, A. Vecchio, G. Vedovato, J. Veitch, P. J. Veitch, K. Venkateswara, G. Venugopalan, D. Verkindt, F. Vetrano, A. Viceré, A. D. Viets, S. Vinciguerra, D. J. Vine, J. Y. Vinet, S. Vitale, T. Vo, H. Vocca, C. Vorvick, S. P. Vyatchanin, A. R. Wade, L. E. Wade, M. Wade, R. Walet, M. Walker, L. Wallace, S. Walsh, G. Wang, H. Wang, J. Z. Wang, W. H. Wang, Y. F. Wang, R. L. Ward, J. Warner, M. Was, J. Watchi, B. Weaver, L. W. Wei, M. Weinert, A. J. Weinstein, R. Weiss, L. Wen, E. K. Wessel, P. Weßels, J. Westerweck, T. Westphal, K. Wette, J. T. Whelan, S. E. Whitcomb, B. F. Whiting, C. Whittle, D. Wilken, D. Williams, R. D. Williams, A. R. Williamson, J. L. Willis, B. Willke, M. H. Wimmer, W. Winkler, C. C. Wipf, H. Wittel, G. Woan, J. Woehler, J. Wofford, K. . W. K. Wong, J. Worden, J. L. Wright, D. S. Wu, D. M. Wysocki, S. Xiao, H. Yamamoto, C. C. Yancey, L. Yang, M. J. Yap, M. Yazback, H. Yu, H. Yu, M. Yvert, A. Zadrożny, M. Zanolin, T. Zelenova, J. P. Zendri,

M. Zevin, L. Zhang, M. Zhang, T. Zhang, Y. H. Zhang, C. Zhao, M. Zhou, Z. Zhou, S. J. Zhu, X. J. Zhu, A. B. Zimmerman, M. E. Zucker, J. Zweizig, (LIGO Scientific Collaboration, Virgo Collaboration, E. Burns, P. Veres, D. Kocevski, J. Racusin, A. Goldstein, V. Connaughton, M. S. Briggs, L. Blackburn, R. Hamburg, C. M. Hui, A. von Kienlin, J. McEnery, R. D. Preece, C. A. Wilson-Hodge, E. Bissaldi, W. H. Cleveland, M. H. Gibby, M. M. Giles, R. M. Kippen, S. McBreen, C. A. . Meegan, W. S. Paciesas, S. Poolakkil, O. J. Roberts, M. Stanbro, F. Gamma-ray Burst Monitor, V. Savchenko, C. Ferrigno, E. Kuulkers, A. Bazzano, E. Bozzo, S. Brandt, J. Chenevez, T. J. L. Courvoisier, R. Diehl, A. Domingo, L. Hanlon, E. Jourdain, P. Laurent, F. Lebrun, A. Lutovinov, S. Mereghetti, L. Natalucci, J. Rodi, J. P. Roques, R. Sunyaev, P. Ubertini, and (INTEGRAL, "Gravitational Waves and Gamma-Rays from a Binary Neutron Star Merger: GW170817 and GRB 170817A," *ApJ*, vol. 848, no. 2, p. L13, Oct. 2017, doi: 10.3847/2041-8213/aa920c.

[4] R. A. Hulse and J. H. Taylor, "Discovery of a pulsar in a binary system." *ApJ*, vol. 195, pp. L51–L53, Jan. 1975.

[5] J. H. Taylor and J. M. Weisberg, "A new test of general relativity - Gravitational radiation and the binary pulsar PSR 1913+16," *ApJ*, vol. 253, pp. 908–920, Feb. 1982.

[6] L. S. Collaboration and J. Aasi, "Advanced ligo," *Class. Quantum Gravity*, vol. 32, no. 7, p. 074001, 2015.

[7] F. a. Acernese, M. Agathos, K. Agatsuma, D. Aisa, N. Allemandou, A. Allocca, J. Amarni, P. Astone, G. Balestri, G. Ballardin *et al.*, "Advanced virgo: a second-generation interferometric gravitational wave detector," *Classical and Quantum Gravity*, vol. 32, no. 2, p. 024001, 2014.

[8] T. A. Prince, M. Tinto, S. L. Larson, and J. W. Armstrong, "LISA optimal sensitivity," *Phys. Rev. D*, vol. 66, no. 12, p. 122002, Dec. 2002, doi: 10.1103/PhysRevD.66.122002.

[9] T. Robson, N. J. Cornish, and C. Liu, "The construction and use of LISA sensitivity curves," *Classical and Quantum Gravity*, vol. 36, no. 10, p. 105011, May 2019, doi: 10.1088/1361-6382/ab1101.

[10] J. R. Gair, S. Babak, A. Sesana, P. Amaro-Seoane, E. Barausse, C. P. L. Berry, E. Berti, and C. Sopuerta, "Prospects for observing extreme-mass-ratio inspirals with LISA," in *Journal of Physics Conference Series*, ser. Journal of Physics Conference Series, vol. 840, May 2017, p. 012021.

[11] A. Klein, E. Barausse, A. Sesana, A. Petiteau, E. Berti, S. Babak, J. Gair, S. Aoudia, I. Hinder, F. Ohme, and B. Wardell, "Science with the space-based interferometer eLISA: Supermassive black hole binaries," *Phys. Rev. D*, vol. 93, no. 2, p. 024003, Jan. 2016.

[12] C. E. A. Chapman-Bird, C. P. L. Berry, and G. Woan, "Rapid determination of LISA sensitivity to extreme mass ratio inspirals with machine learning," *arXiv e-prints*, p. arXiv:2212.06166, Dec. 2022.

[13] T. Wagg, F. S. Broekgaarden, S. E. de Mink, L. A. C. van Son, N. Frankel, and S. Justham, "Gravitational wave sources in our Galactic backyard: Predictions for BHBH, BHNS and NSNS binaries detectable with LISA," *arXiv e-prints*, Nov. 2021, arXiv: 2111.13704.

[14] M. C. Digman and C. M. Hirata, "LISA Galactic Binaries in the Roman Galactic Bulge Time-Domain Survey," *arXiv e-prints*, p. arXiv:2212.14887, Dec. 2022.

[15] V. Korol, E. M. Rossi, and P. J. Groot, "Detection of Double White Dwarf Binaries with Gaia, LSST and eLISA," in *20th European White Dwarf Workshop*, ser. Astronomical Society of the Pacific Conference Series, P. E. Tremblay, B. Gaensicke, and T. Marsh, Eds., vol. 509, Mar. 2017, p. 529.

[16] G. Nelemans, L. R. Yungelson, and S. F. Portegies Zwart, "The gravitational wave signal from the Galactic disk population of binaries containing two compact objects," *A&A*, vol. 375, pp. 890–898, Sep. 2001.

[17] B. Willems, V. Kalogera, A. Vecchio, N. Ivanova, F. A. Rasio, J. M. Fregeau, and K. Belczynski, "Eccentric Double White Dwarfs as LISA Sources in Globular Clusters," *ApJ*, vol. 665, no. 1, pp. L59–L62, Aug. 2007.

[18] A. J. Ruiter, K. Belczynski, M. Benacquista, S. L. Larson, and G. Williams, "The LISA Gravitational Wave Foreground: A Study of Double White Dwarfs," *ApJ*, vol. 717, no. 2, pp. 1006–1021, Jul. 2010.

[19] M. Y. M. Lau, I. Mandel, A. Vigna-Gómez, C. J. Neijssel, S. Stevenson, and A. Sesana, "Detecting

double neutron stars with LISA," *MNRAS*, vol. 492, no. 3, pp. 3061–3072, Mar. 2020, doi: 10.1093/mnras/staa002.

[20] A. Sesana, M. Volonteri, and F. Haardt, "LISA detection of massive black hole binaries: imprint of seed populations and extreme recoils," *Classical and Quantum Gravity*, vol. 26, no. 9, p. 094033, May 2009, doi: 10.1088/0264-9381/26/9/094033.

[21] Z. Khakhaleva-Li and C. J. Hogan, "Will LISA Detect Harmonic Gravitational Waves from Galactic Cosmic String Loops?" *arXiv*, May 2020, arXiv: 2006.00438.

[22] M. Renzo, T. Callister, K. Chatziioannou, L. A. C. van Son, C. M. F. Mingarelli, M. Cantiello, K. E. S. Ford, B. McKernan, and G. Ashton, "Prospects of Gravitational Wave Detections from Common Envelope Evolution with LISA," *ApJ*, vol. 919, no. 2, p. 128, Oct. 2021, doi: 10.3847/1538-4357/ac1110.

[23] J. Fumagalli, M. Pieroni, S. Renaux-Petel, and L. T. Witkowski, "Detecting primordial features with LISA," *JCAP*, vol. 2022, no. 7, p. 020, Jul. 2022, doi: 10.1088/1475-7516/2022/07/020.

[24] F. S. Broekgaarden, E. Berger, C. J. Neijssel, A. Vigna-Gómez, D. Chattopadhyay, S. Stevenson, M. Chruslinska, S. Justham, S. E. de Mink, and I. Mandel, "Impact of massive binary star and cosmic evolution on gravitational wave observations I: black hole-neutron star mergers," *MNRAS*, vol. 508, no. 4, pp. 5028–5063, Dec. 2021, doi: 10.1093/mnras/stab2716.

[25] Y. Shao and X.-D. Li, "Population Synthesis of Black Hole Binaries with Compact Star Companions," *ApJ*, vol. 920, no. 2, p. 81, Oct. 2021, doi: 10.3847/1538-4357/ac173e.

[26] J. J. Andrews, K. Breivik, C. Pankow, D. J. D'Orazio, and M. Safarzadeh, "LISA and the Existence of a Fast-merging Double Neutron Star Formation Channel," *ApJ*, vol. 892, no. 1, p. L9, Mar. 2020, doi: 10.3847/2041-8213/ab5b9a.

[27] K. Belczynski, M. Benacquista, and T. Bulik, "Double Compact Objects as Low-frequency Gravitational Wave Sources," *ApJ*, vol. 725, no. 1, pp. 816–823, Dec. 2010, doi: 10.1088/0004-637X/725/1/816.

[28] H.-K. Guo, J. Shu, and Y. Zhao, "Using LISA-like Gravitational Wave Detectors to Search for Primordial Black Holes," *arXiv e-prints*, p. arXiv:1709.03500, Sep. 2017.

[29] S. Babak, J. G. Baker, M. J. Benacquista, N. J. Cornish, S. L. Larson, I. Mandel, S. T. McWilliams, A. Petiteau, E. K. Porter, E. L. Robinson, M. Vallisneri, A. Vecchio, t. M. L. Data Challenge Task Force, M. Adams, K. A. Arnaud, A. Błaut, M. Bridges, M. Cohen, C. Cutler, F. Feroz, J. R. Gair, P. Graff, M. Hobson, J. Shapiro Key, A. Królak, A. Lasenby, R. Prix, Y. Shang, M. Trias, J. Veitch, J. T. Whelan, and t. C. . participants, "The Mock LISA Data Challenges: from challenge 3 to challenge 4," *Classical and Quantum Gravity*, vol. 27, no. 8, p. 084009, apr 2010.

[30] A. Błaut, S. Babak, and A. Królak, "Mock LISA data challenge for the Galactic white dwarf binaries," *Phys. Rev. D*, vol. 81, no. 6, p. 063008, mar 2010.

[31] S. Babak, J. G. Baker, M. J. Benacquista, N. J. Cornish, J. Crowder, C. Cutler, S. L. Larson, T. B. Littenberg, E. K. Porter, M. Vallisneri, A. Vecchio, t. M. L. data challenge task force, G. Auger, L. Barack, A. Błaut, E. Bloomer, D. A. Brown, N. Christensen, J. Clark, S. Fairhurst, J. R. Gair, H. Halloin, M. Hendry, A. Jimenez, A. Królak, I. Mandel, C. Messenger, R. Meyer, S. Mohanty, R. Nayak, A. Petiteau, M. Pitkin, E. Plagnol, R. Prix, E. L. Robinson, C. Roever, P. Savov, A. Stroeer, J. Toher, J. Veitch, J. Vinet, L. Wen, J. T. Whelan, G. Woan, and t. Challenge-2 participants, "Report on the second Mock LISA data challenge," *Classical and Quantum Gravity*, vol. 25, no. 11, p. 114037, jun 2008.

[32] S. Yu and C. S. Jeffery, "The gravitational wave signal from diverse populations of double white dwarf binaries in the Galaxy," *A&A*, vol. 521, p. A85, Oct. 2010.

[33] T. Wagg, K. Breivik, and S. E. de Mink, "LEGWORK: A Python Package for Computing the Evolution and Detectability of Stellar-origin Gravitational-wave Sources with Space-based Detectors," *ApJS*, vol. 260, no. 2, p. 52, Jun. 2022, doi: 10.3847/1538-4365/ac5c52.

[34] S. Stevenson, A. Vigna-Gómez, I. Mandel, J. W. Barrett, C. J. Neijssel, D. Perkins, and S. E. de Mink, "Formation of the first three gravitational-wave observations through isolated binary evolution," *Nat.*

Commun., vol. 8, p. 14906, Apr. 2017, doi: 10.1038/ncomms14906.

[35] J. Riley, P. Agrawal, J. W. Barrett, K. N. K. Boyett, F. S. Broekgaarden, D. Chattopadhyay, S. M. Gaebel, F. Gittins, R. Hirai, G. Howitt, S. Justham, L. Khandelwal, F. Kummer, M. Y. M. Lau, I. Mandel, S. E. de Mink, C. Neijssel, T. Riley, L. van Son, S. Stevenson, A. Vigna-Gómez, S. Vinciguerra, T. Wagg, R. Willcox, and Team Compas, "Rapid Stellar and Binary Population Synthesis with COMPAS," *ApJS*, vol. 258, no. 2, p. 34, Feb. 2022, doi: 10.3847/1538-4365/ac416c.

[36] A. Vigna-Gómez, C. J. Neijssel, S. Stevenson, J. W. Barrett, K. Belczynski, S. Justham, S. E. de Mink, B. Müller, P. Podsiadlowski, M. Renzo, D. Szécsi, and I. Mandel, "On the formation history of Galactic double neutron stars," *MNRAS*, vol. 481, no. 3, pp. 4009–4029, Dec. 2018.

[37] J. R. Hurley, O. R. Pols, and C. A. Tout, "Comprehensive analytic formulae for stellar evolution as a function of mass and metallicity," *MNRAS*, vol. 315, no. 3, pp. 543–569, Jul. 2000.

[38] J. R. Hurley, C. A. Tout, and O. R. Pols, "Evolution of binary stars and the effect of tides on binary populations," *MNRAS*, vol. 329, no. 4, pp. 897–928, Feb. 2002.

[39] P. Kroupa, "On the variation of the initial mass function," *MNRAS*, vol. 322, no. 2, pp. 231–246, Apr. 2001, doi: 10.1046/j.1365-8711.2001.04022.x.

[40] H. Sana, S. E. de Mink, A. de Koter, N. Langer, C. J. Evans, M. Gieles, E. Gosset, R. G. Izzard, J. B. Le Bouquin, and F. R. N. Schneider, "Binary Interaction Dominates the Evolution of Massive Stars," *Science*, vol. 337, no. 6093, p. 444, Jul. 2012, doi: 10.1126/science.1223344.

[41] E. Öpik, "Statistical Studies of Double Stars: On the Distribution of Relative Luminosities and Distances of Double Stars in the Harvard Revised Photometry North of Declination -31°," *Publications of the Tartu Astrofizica Observatory*, vol. 25, p. 1, Jan. 1924.

[42] C. L. Fryer, K. Belczynski, G. Wiktorowicz, M. Dominik, V. Kalogera, and D. E. Holz, "Compact Remnant Mass Function: Dependence on the Explosion Mechanism and Metallicity," *ApJ*, vol. 749, no. 1, p. 91, apr 2012.

[43] I. Mandel and B. Müller, "Simple recipes for compact remnant masses and natal kicks," *MNRAS*, vol. 499, no. 3, pp. 3214–3221, dec 2020.

[44] P. C. Peters and J. Mathews, "Gravitational Radiation from Point Masses in a Keplerian Orbit," *Physical Review*, vol. 131, no. 1, pp. 435–440, Jul. 1963, doi: 10.1103/PhysRev.131.435.

[45] P. C. Peters, "Gravitational Radiation and the Motion of Two Point Masses," *Physical Review*, vol. 136, no. 4B, pp. 1224–1232, Nov. 1964, doi: 10.1103/PhysRev.136.B1224.

[46] L. S. Finn and K. S. Thorne, "Gravitational waves from a compact star in a circular, inspiral orbit, in the equatorial plane of a massive, spinning black hole, as observed by LISA," *Phys. Rev. D*, vol. 62, no. 12, p. 124021, Dec. 2000, doi: 10.1103/PhysRevD.62.124021.

[47] L. Barack and C. Cutler, "LISA capture sources: Approximate waveforms, signal-to-noise ratios, and parameter estimation accuracy," *Phys. Rev. D*, vol. 69, no. 8, p. 082005, Apr. 2004, doi: 10.1103/PhysRevD.69.082005.

[48] F. S. Broekgaarden, S. Justham, S. E. de Mink, J. Gair, I. Mandel, S. Stevenson, J. W. Barrett, A. Vigna-Gómez, and C. J. Neijssel, "STROOPWAFEL: simulating rare outcomes from astrophysical populations, with application to gravitational-wave sources⋆," *MNRAS*, vol. 490, no. 4, pp. 5228–5248, Dec. 2019.

[49] J. W. Barrett, S. M. Gaebel, C. J. Neijssel, A. Vigna-Gómez, S. Stevenson, C. P. L. Berry, W. M. Farr, and I. Mandel, "Accuracy of inference on the physics of binary evolution from gravitational-wave observations," *MNRAS*, vol. 477, no. 4, pp. 4685–4695, Jul. 2018.

[50] N. Frankel, H.-W. Rix, Y.-S. Ting, M. Ness, and D. W. Hogg, "Measuring Radial Orbit Migration in the Galactic Disk," *ApJ*, vol. 865, no. 2, p. 96, Oct. 2018, doi: 10.3847/1538-4357/aadba5.

[51] J. Bovy, H. W. Leung, J. A. S. Hunt, J. T. Mackereth, D. A. García-Hernández, and A. Roman-Lopes, "Life in the fast lane: a direct view of the dynamics, formation, and evolution of the Milky Way's bar," *MNRAS*, vol. 490, no. 4, pp. 4740–4747, Dec. 2019, doi: 10.1093/mnras/stz2891.

[52] P. J. McMillan, "Mass models of the Milky Way," *MNRAS*, vol. 414, no. 3, pp. 2446–2457, Jul. 2011, doi: 10.1111/j.1365-2966.2011.18564.x.

[53] J. Bovy, H.-W. Rix, E. F. Schlafly, D. L. Nidever, J. A. Holtzman, M. Shetrone, and T. C. Beers, "The Stellar Population Structure of the Galactic Disk," *ApJ*, vol. 823, no. 1, p. 30, May 2016, doi: 10.3847/0004-637X/823/1/30.

[54] C. Wegg, O. Gerhard, and M. Portail, "The structure of the Milky Way's bar outside the bulge," *MNRAS*, vol. 450, no. 4, pp. 4050–4069, Jul. 2015.

APPENDIX A
SETTINGS FOR USING COMPAS

To generate a binary systems, COMPAS requires the following parameters from the user as discussed earlier,

- mass of primary star $(m_{1_{\text{ZAMS}}})$,
- mass of secondary star $(m_{2_{\text{ZAMS}}})$,
- semi-major axis of the orbit (a_{ZAMS}),
- random seed $(\varnothing)$
- remnant mass prescription,
- eccentricity of the orbit (e_{ZAMS}), and
- metallicity of the stars (Z).

We've discussed the first four parameters in the main text, here we will discuss the selection of eccentricity and metallicity values.

ECCENTRICITY

In order to evaluate whether the initial eccentricity affects GW emission at the end stages of the DCO, we generate two identical data sets. For the primary data set, we chose the eccentricity value to be varied between 0 and 1. For the selection of eccentricity, the power law and gamma distribution were also considered.

A. Power law distribution

The random values for metallicity were generated using the power law distribution given below,

$$f(x, a) = ax^{(a-1)} \tag{7}$$

where a is the index of the power law distribution.[5] Figure 6 shows the plot for the probability density function (PDF) of the power law with $a \in [1, 2]$. Although the distribution can produce higher values, it does not suppress the lower values so this distribution was discarded.

B. Gamma distribution

For the probability density function for gamma distribution,[6] we use the following form,

$$f(x, a) = \frac{x^{a-1}\exp(-x)}{\Gamma(a)} \tag{8}$$

for $x \geq 0$ and $a > 0$. Here, a is the shape factor, and Γ is the gamma function, such that $\Gamma(a) = (a-1)!$. Similar to the power law distribution, the gamma distribution (see, figure 7) was not a good selection for the values of metallicity that were required for this study.

C. Beta distribution

For the beta distribution, we use the following form,

$$f(x, a, b) = \frac{\Gamma(a+b)x^{a-1}(1-x)^{b-1}}{\Gamma(a)\Gamma(b)} \tag{9}$$

For $0 \leq x \leq 1, a > 0, b > 0$ and Γ is the gamma function.[7]

[5] https://docs.scipy.org/doc/scipy/reference/generated/scipy.stats.powerlaw.html
[6] https://docs.scipy.org/doc/scipy/reference/generated/scipy.stats.gamma.html
[7] https://docs.scipy.org/doc/scipy/reference/generated/scipy.stats.beta.html

Figure 8 shows the beta distribution with a fixed $\beta = 80$. Similarly, figure 9 shows the beta distribution with a fixed $\alpha = 5$. For our case, we selected Beta$(5, 80)$ as our distribution of choice for metallicity and generated 10^7 values between the COMPAS limits $10^{-4} < z < 0.03$.

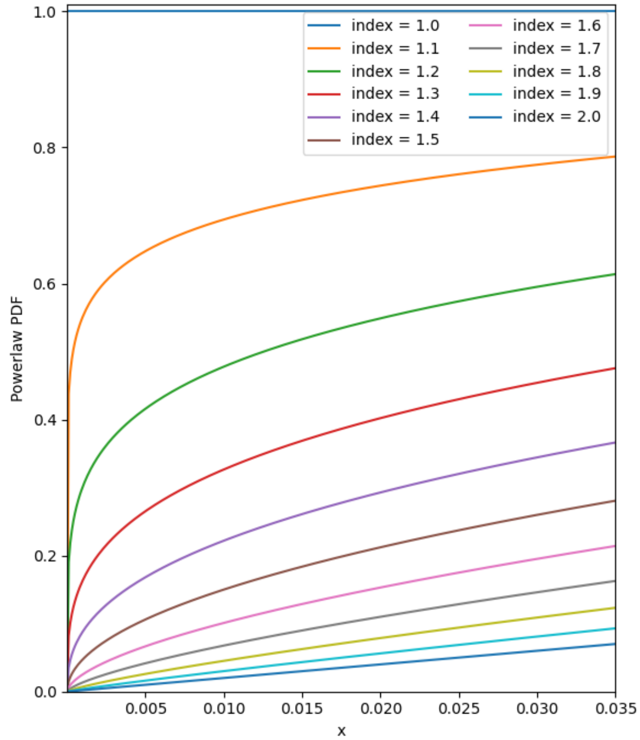

Fig. 6: Power-law distribution

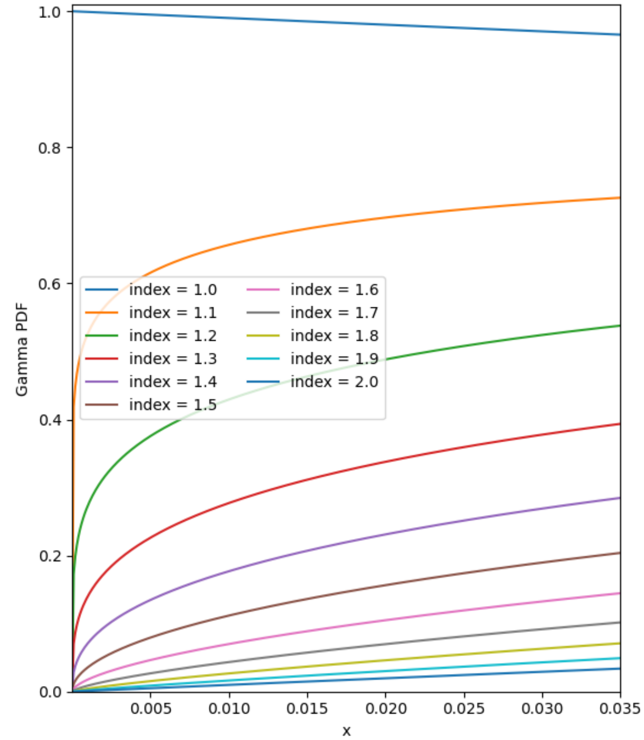

Fig. 7: Gamma distribution

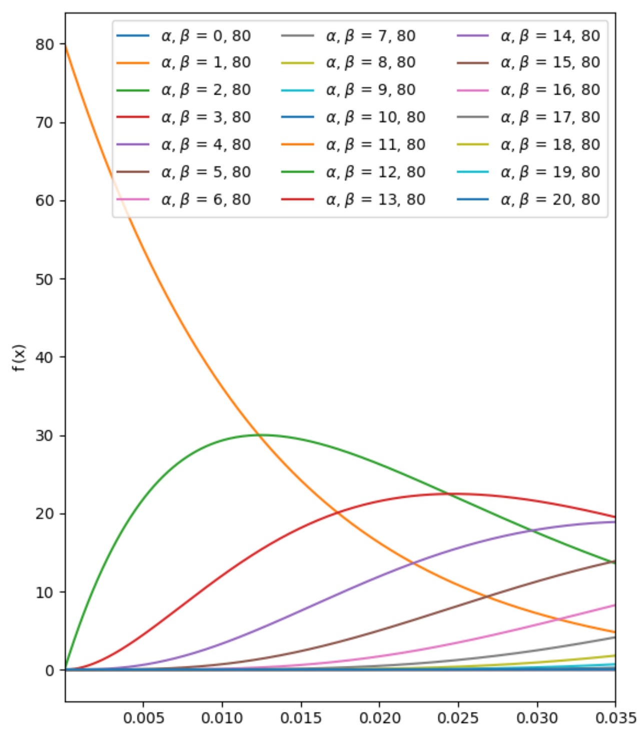

Fig. 8: Beta distribution with varying α and fixed β parameter.

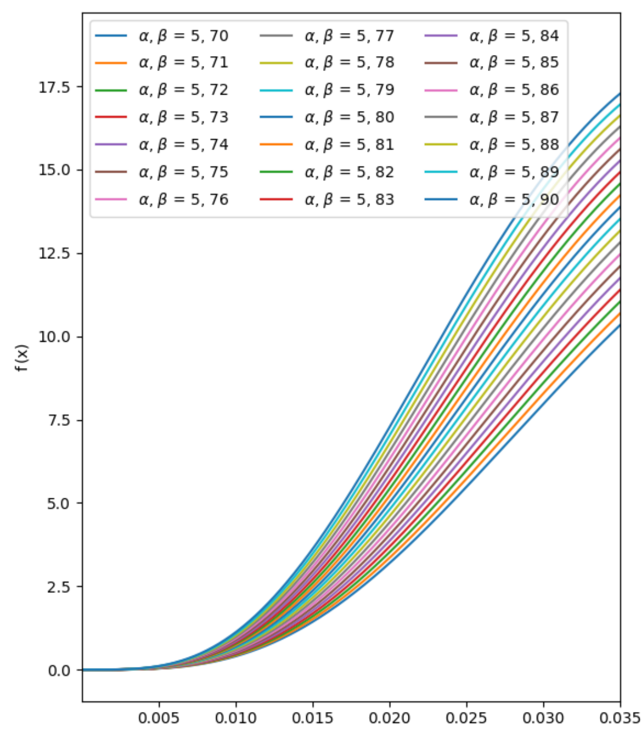

Fig. 9: Beta distribution with fixed α and varying β parameter.

METALLICITY

One of the major challenges in generation of the stellar binaries for this study was the selection of a distribution which will result in stars at the higher end of COMPAS metallicity boundary, $z = 0.03$. A power-law, gamma, and beta distributions were selected to try and simulate the required metallicity distribution. In the following section, we discuss the selected distributions briefly,

APPENDIX B
MILKY WAY MODEL

In this section, we will briefly outline the milky way galaxy model used in this study. The model is developed by [13] and makes use of the galaxy's enrichment history by taking into account the metallicity-radius-time relationship [50]. It uses a separate star formation history and spatial distribution for the low-[α/Fe], high-[α/Fe] discs, and bulge in the galaxy.

A. Star formation rate

The star formation rate for both the low-[α/Fe] and high-[α/Fe] disks is expressed as,

$$p(\tau) \propto \exp\left(-\frac{\tau_m - \tau}{\tau_{\text{SFR}}}\right), \tag{10}$$

where τ is the time difference between the star's ZAMS stage and today. The age of milky way galaxy, τ_m, is taken as $12\,\text{Gyr}$, and the star formation rate as, $\tau_{\text{SFR}} = 6.8\,\text{Gyr}$. The star-forming period of low-[α/Fe] and high-[α/Fe] discs were taken as $0\,\text{Gyr}$ to $8\,\text{Gyr}$ and $8\,\text{Gyr}$ to $12\,\text{Gyr}$ respectively. The model adopts $6\,\text{Gyr}$ to $12\,\text{Gyr}$ as the star-forming period of the bulge [51].

B. Radial distribution

The radial distribution of stars within the milky way galaxy was performed using the following expression,

$$p(R) = \exp\left(-\frac{R}{R_d}\right)\frac{R}{R_d^2} \tag{11}$$

However, a different scale length, R_d, was chosen for each component of the galaxy. For low-[α/Fe], the model uses $R_{\text{exp}}(\tau)$ as the scale length [50, Eq 6], where

$$R_{\text{exp}}(\tau) = 4\,\text{kpc}\left[1 - \alpha_{R_{\text{exp}}}\left(\frac{\tau}{8\,\text{Gyr}}\right)\right], \tag{12}$$

with the value of inside-out growth parameter, $\alpha_{R_{\text{exp}}}$, as 0.3. For high-[α/Fe] disc and bulge, the value of scale length was chosen as $(1/0.43)\,\text{kpc}$ and $1.5\,\text{kpc}$ respectively.

C. Vertical distribution

The model employs a similar method of single exponent expression with varying scale height parameters for the vertical distribution as well. The exponential expression used is,

$$p(|z|) = \frac{1}{z_d}\exp\left(-\frac{z}{z_d}\right), \tag{13}$$

where z here is the vertical displacement from the galactic plane. The scale height parameter, z_d, for low-[α/Fe], high-[α/Fe] and bulge was taken as $0.3\,\text{kpc}$ [52], $0.95\,\text{kpc}$ [53], and $0.2\,\text{kpc}$ [54] respectively.

D. Metallicity-radius-time relationship

The MRT relationship plays an important part, both in the galaxy model and later on in the placement of DCOs within the galaxy as well. The model makes use of [50, Eq. 7],

$$[\text{Fe/H}](R,\tau) = F_m + \nabla[\text{Fe/H}]R - \left(F_m + \nabla[\text{Fe/H}]R^{\text{now}}_{[\text{Fe/H}]=0}\right)f(\tau) \tag{14}$$

For each point generated, if the value of metallicity produced by the MW model was less or greater than the limits defined by COMPAS[8] it was changed to a uniformly drawn random number between $\text{COMPAS}_{\text{min}} - \text{ZSOLAR}$ and $\text{ZSOLAR} - \text{COMPAS}_{\text{max}}$ respectively.

[8] 0.0001, 0.03

E. Galaxy synthesis

For the synthesis of an instance of the Milky Way galaxy, the model described previously samples the following parameters,

$$\theta_i = \{\tau, D, z, \text{component}\},$$

where τ is the look-back time for the binary, D is the distance from Earth, z is the metallicity, and 'component' is the component of the galaxy in which the binary resides.[9] The parameters are generated for $i = 1, 2, 3, \ldots,$ N_{GAL}, where $N_{\mathrm{GAL}} = 100$.

[9]One of the three, low-[α/Fe] disc, high-[α/Fe] disc, or bulge.